Advances in Aircraft and Spacecraft Science, *Vol. 2, No. 2 (2015) 183-198*
DOI: http://dx.doi.org/10.12989/aas.2015.2.2.183

Thrust augmentation through after-burning in scramjet nozzles

Michael J. Candon*, Hideaki Ogawa[a] and Graham E. Dorrington[b]

School of Aerospace, Mechanical and Manufacturing Engineering, RMIT University, GPO Box 2476, Melbourne, VIC 3001, Australia

(Received September 24, 2014, Revised November 6, 2014, Accepted November 22, 2014)

Abstract. Scramjets are a class of hypersonic airbreathing engine that are associated with realizing the technology required for economical, reliable access-to-space and high-speed atmospheric transport. After-burning augments the thrust produced by the scramjet nozzle and creates a more robust nozzle design. This paper presents a numerical study of three parameters and the effect that they have on thrust augmentation. These parameters include the injection pressure, injection angle and streamwise injection position. It is shown that significant levels of thrust augmentation are produced based upon contributions from increased pressure, mass flow and energy in the nozzle. Further understanding of the phenomenon by which thrust augmentation is being produced is provided in the form of a force contribution breakdown, analysis of the nozzle flowfields and finally the analysis of the surface pressure and shear stress distributions acting upon the nozzle wall.

Keywords: after-burning; combustion; CFD; hypersonic flow; nozzle; scramjet

1. Introduction

The development of hypersonic airbreathing engines is of great interest in space transportation as they provide an economically sound, reusable and high-speed platform for the transport of both civilians and cargo from the Earth to the low Earth orbit (Froning 1989). Scramjet (supersonic combustion ramjet) propulsion is a promising hypersonic airbreathing technology which eliminates the need to carry an oxidizer and offers higher specific impulse than conventional rocket engines. Significant progress has been made in the development of scramjet technology over the last decade, with projects including NASA's Hyper-X program (McClinton 2006) and the flight of the Boeing X-51A WaveRider in May 2010 (Mutzman and Murphy 2011). A scramjet cycle demonstrated in Fig. 1 involves an intake of hypersonic air which is compressed to high pressure and temperature, fuel is then injected and combusted supersonically in the combustion chamber and the exhaust gas is expanded through the nozzle, resulting in net thrust.

The expanding exhaust gas comprises of a significant proportion of unburned hydrogen which under ideal conditions can be combusted via the injection of liquid oxygen directly into the unburned hydrogen stream, i.e., by introducing after-burning. This has the potential to significantly

*Corresponding author, Undergraduate, E-mail: s3329364@student.rmit.edu.au
[a]Senior Research Fellow, E-mail: hideaki.ogawa@rmit.edu.au
[b]Senior Lecturer, E-mail: graham.dorrington@rmit.edu.au

Copyright © 2015 Techno-Press, Ltd.
http://www.techno-press.org/?journal=aas&subpage=7 ISSN: 2287-528X (Print), 2287-5271 (Online)

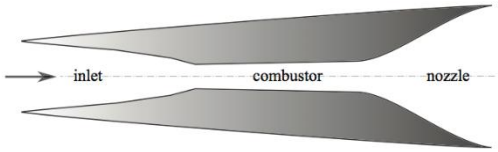

Fig. 1 Schematic of axisymmetric scramjet engine with flow direction (Ogawa and Boyce 2012)

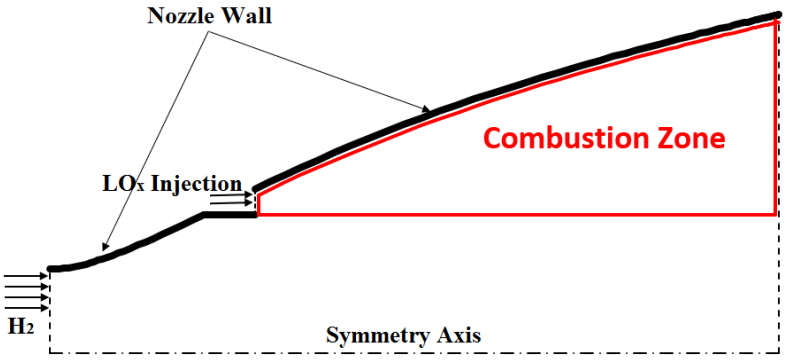

Fig. 2 Schematic of the scramjet after-burning scheme (injector not to scale)

increase the thrust produced by the nozzle whilst also maintaining an ideal nozzle expansion ratio (p_{exit}=p_{atm}) (Davies 2003) by decreasing the injection pressure of liquid oxygen as the flight altitude increases. A schematic of the after-burning scheme is presented in Fig. 2.

There are several critical factors that must be considered with such an after-burning scheme including mixing of reactants, ignition and completion of combustion. The phenomena that are associated with supersonic combustion also introduce several difficulties into the supersonic flowfield such as turbulent mixing, shock interaction and heat release (Ferri *et al.* 1965, Pandey and Sivasakthivel 2011, Papamoschu and Roshko 1986). The ramp-injector configuration shown in Fig. 2 allows efficient mixing with near streamwise injection which minimizes losses due to low pressure gradients downstream of shocks induced by an injection angle. The ramp also provides a region for flame holding and flame stabilisation through the buildup of a radical pool. However the benefits of a ramp injector remain provided that the geometry does not result in too severe a local flow disturbance as this may result in pressure losses as well as more demanding wall cooling requirements (Cutler *et al.* 2001, Drummond *et al.* 1991, Drummond *et al.* 2006).

The scheme envisaged is effectively a combined-cycle scramjet rocket, or ejector scramjet. Whilst thrust is augmented substantially, specific impulse falls as the liquid oxygen injection rate increases. Similar after-burning schemes have been proposed and/or tested for rocket engines without any air-breathing. These include Supersonic After-Burning Rocket Engine (SABRE) (Dorrington 2002) and Thrust Augmented Nozzle (TAN) (Bulman 2006, Ferrante and Chen 2006, Forde *et al.* 2006). TAN is a scheme introduced by GenCorp Aerojet in 2006 in which numerical simulations and physical testing were conducted on a thrust augmented nozzle which involved hydrogen-oxygen combustion upstream of the rocket nozzle throat. It was found that a significant level of thrust augmentation was achieved, attributed to increased mass flow, inertia and energy in the nozzle resulting from the TAN injection propellants. Further, they were able to eliminate thrust

penalties due to over expansion of the nozzle. TAN considered the injection of both fuel and oxidizer in order to augment thrust; this led to efficient combustion adjacent to the nozzle wall upstream of the TAN injectors. If a similar injection scheme were to be introduced in scramjet after-burning it would eliminate the limitations associated with supersonic mixing and the inherent effect on combustion.

This paper builds upon research conducted by Ogawa and Boyce (2012) who considered the design optimization of an axisymmetric scramjet nozzle for the SCRAMSPACE project conducted by The University of Queensland (Boyce *et al.* 2011), the optimized geometry acts as the baseline geometry for the present study. The optimization of the nozzle contour was based upon nozzle inflow conditions that were obtained from a separate CFD simulation in which the scramjet intake and combustor were included. The nozzle inflow therefore contained reacted gases and for the present study these nozzle inflow conditions remain unaltered.

The optimized geometry obtained by Ogawa and Boyce (2012) is adapted by including the injection of liquid oxygen via the ramp configuration. The influence of several parameters on thrust augmentation is investigated including the injection pressure, streamwise injection position and injection angle. The streamwise injection position influences the mixing and combustion time significantly. Further, the position of the injector should be such that temperatures and pressures of the crossflow are sufficiently high promoting, sufficient fast combustion (Ferri *et al.* 1965). As the injection angle increases, enhanced penetration, mixing and combustion occurs. However, higher injection angles lead to intensified levels of interactions between the injected oxygen and the crossflow, causing upstream and downstream wall flow separation and increased wall static temperatures. The injection pressure influences the penetration levels of the fuel jet such that higher pressure leads to higher levels of penetration and allows for enhanced mixing and combustion. The momentum produced by the injected oxygen also directly influences the augmentation of thrust and higher injection pressures yield a greater momentum increase. The highly complex nature of the scramjet nozzle flowfield suggests that it is imperative to optimize the aforementioned injection parameters in order to promote maximum thrust augmentation.

2. Methods

2.1 Conditions and configurations

2.1.1 Nozzle configuration

The axisymmetric scramjet engine being considered in this study is based on the SCRAMSPACE configuration (Boyce *et al.* 2011). The scramjet has 20 design parameters in total. Fig. 3 presents the configuration of the entire scramjet engine with all 20 parameters indicated to define the angle, length and curvature of the components.

The optimization conducted by Ogawa and Boyce (2012) considered the nozzle entrance position in the axial direction and the nozzle radius fixed at 0.808 m and 0.0351 m respectively which remains unaltered. Fig. 4 demonstrates the optimized nozzle geometry that is considered for this study.

A ramp injector is introduced to the geometry which tapers away from the optimum nozzle contour until the injection position x_j is reached and the ramp drops off vertically according to the magnitude of the injector height h_j. The operating conditions and configurations of the injector are presented in Section 2.3.

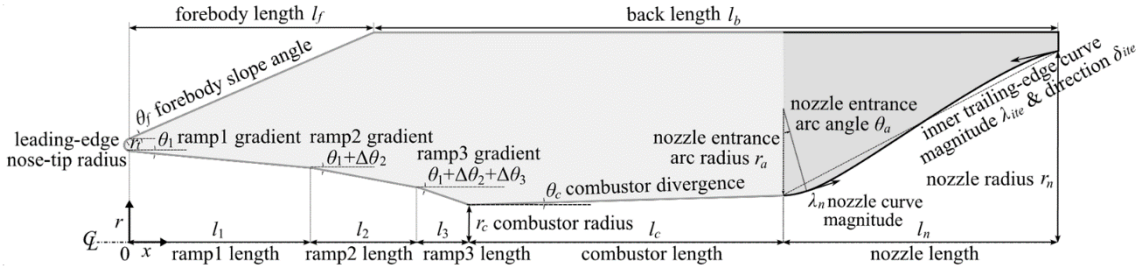

Fig. 3 Parametric representation of the scramjet geometry

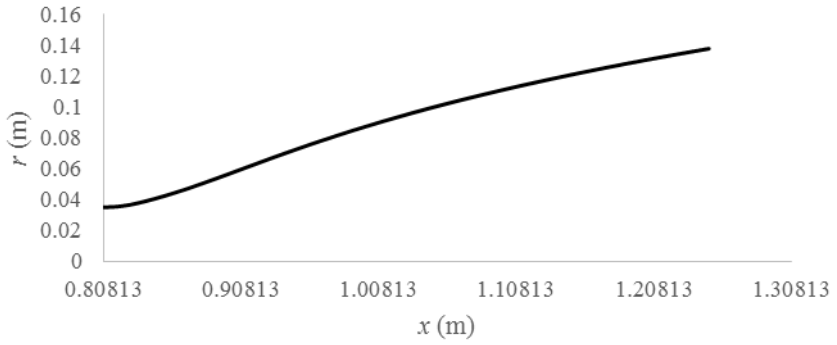

Fig. 4 Contour of optimum nozzle geometry

Table 1 Freestream conditions of design points for cruise at M_∞=8

Altitude H (km)	Velocity u_∞ (m/s)	Static Pressure p_∞ (Pa)	Static Temperature T_∞ (K)	Dynamic Pressure q_∞ (kPa)	Reynolds Number Re_∞
27	2425	1847	223.7	82.5	3.53×10^5

2.1.2 Freestream conditions

This study considers cruise conditions at an altitude of 27 km with the scramjet in operation at Mach 8. Table 1 demonstrates the freestream conditions that are implemented, where the Reynolds number is based on the inlet capture radius of 0.075 m.

2.2 Computational fluid dynamics

2.2.1 Flow solver

The flowfields for the scramjet nozzle are computed using ANSYS Fluent, a commercial CFD code that includes detailed turbulence modeling and demonstrates accuracy in computing complex reactions and the occurrence of shocks, making it a suitable choice for hypersonic aerodynamics and supersonic combustion (Maicke and Majdalani 2010). The Navier-Stokes equations for steady flowfields are solved via an implicit algorithm with second order spatial accuracy; higher order term relaxation with a relaxation factor of 0.25 is used to accelerate convergence. Flux vectors are computed according to the Advection Upstream Splitting Method (AUSM), which accurately captures shock discontinuities and has been used in a wide range of problems concerning hypersonic aerodynamics (Manoha *et al*. 2004, Mary and Sagaut 2002). The Evans and

Table 2 Species and reactions for the Evans and Schexnayder supersonic hydrogen combustion model

Species		Reactions			
1	H	1	$HNO_2+M\rightarrow NO+OH+M$	14	$OH+OH\rightarrow H+HO_2$
2	O	2	$NO_2+M\rightarrow NO+O+M$	15	$H_2O+O\rightarrow H+HO_2$
3	H_2O	3	$H_2+M\rightarrow H+H+M$	16	$OH+O_2\rightarrow O+HO_2$
4	OH	4	$O_2+M\rightarrow O+O+M$	17	$H_2O+O_2\rightarrow OH+HO_2$
5	O_2	5	$H_2O+M\rightarrow OH+H+M$	18	$H_2+O_2\rightarrow H+HO_2$
6	H_2	6	$OH+M\rightarrow O+H+M$	19	$O+N_2\rightarrow N+NO$
7	N_2	7	$HO_2+M\rightarrow H+O_2+M$	20	$H+NO\rightarrow N+OH$
8	N	8	$H_2O+O\rightarrow OH+OH$	21	$O+NO\rightarrow N+O_2$
10	NO	9	$H_2O+H\rightarrow OH+H_2$	22	$NO+OH\rightarrow H+NO_2$
11	NO_2	10	$O_2+H\rightarrow OH+O$	23	$NO+O_2\rightarrow O+NO_2$
11	HO_2	11	$H_2+O\rightarrow OH+H$	24	$NO_2+H_2\rightarrow O+NO_2$
12	HNO_2	12	$H_2+O_2\rightarrow OH+OH$	25	$NO_2+OH\rightarrow NO+HO_2$
		13	$H_2+O_2\rightarrow H+HO_2$		

Schexnayder model is used to represent both the reacting exhaust flow and the supersonic hydrogen-oxygen combustion resulting from the oxygen injection which considers 12 species and 25 reactions presented in Table 2 (Evans and Schexnayder 1980).

Both the nozzle and injector inflows are assumed to be fully turbulent and modeled with the two-equation SST *k-ω* RANS model which is a suitable choice according to Chan *et al.* (2012) who demonstrated agreement between numerical and experimental results using the *k-ω* turbulence model for scramjet flowfield simulations. The solution was initialised from freestream conditions with the Explicit Under-Relaxation Factor reduced to 0.5. The CFL number is set to 0.5 for the first 100 iterations and then increased to 5 and run until a converged solution is obtained. The calculation is run for either 1200 iterations, or until the energy residual dropped to 10^{-5} (whichever occurs first).

2.2.2 Computational mesh

In creating the two-dimensional structured mesh, it is ensured that the resolution would be sufficiently fine to capture the boundary layers, shockwaves and reactions accurately, whilst keeping computational time minimal. The geometry and meshes are both constructed using the ANSYS workbench tools; DesignModeler and FLUENT Meshing. A final mesh resolution of 32,350 cells (32,806 nodes) as displayed in Fig. 5 is chosen based on a mesh convergence study which considered a balance between solution accuracy and computational cost. The results of the study are presented in Section 2.2.3. The dimensionless wall distance y^+ ranges from 1.1 to 4.5 along the nozzle wall surface.

2.2.3 Validation and mesh convergence

A simulation incorporating the baseline geometry and nozzle inflow profiles as obtained from Ogawa and Boyce (2012) is utilised for cross-validation purposes. Ogawa and Boyce (2012) solved for the scramjet flowfields with the commercial CFD code CFD++ which is the code utilised in the Australian hypersonics community due to its high fidelity and validation against experimental results. The cross-validation is conducted to ensure that the flowfields being solved

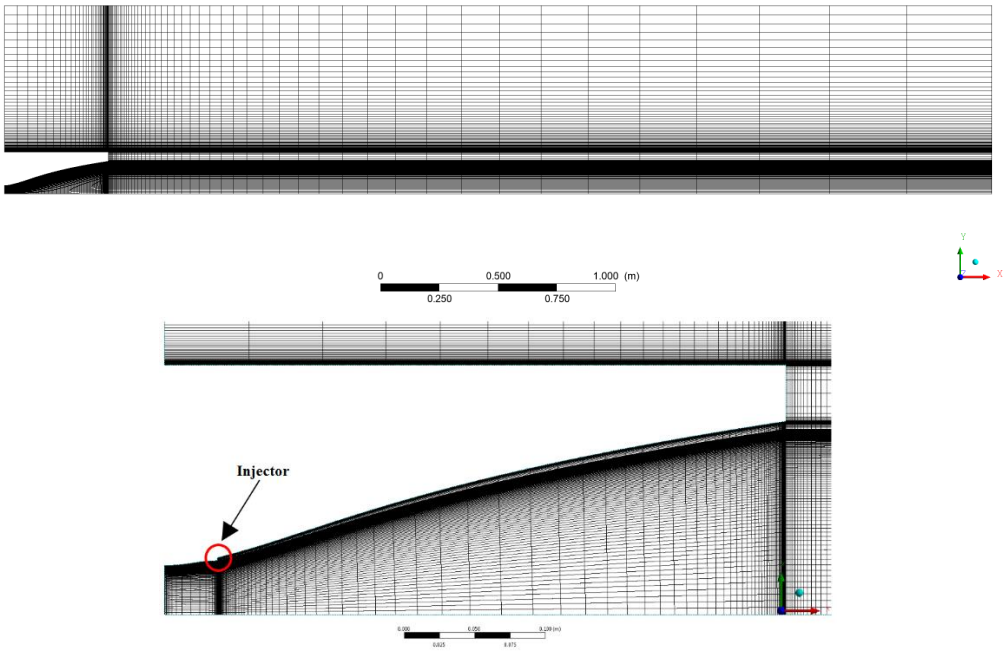

Fig. 5 Computational mesh, full (top) and enhanced nozzle (bottom)

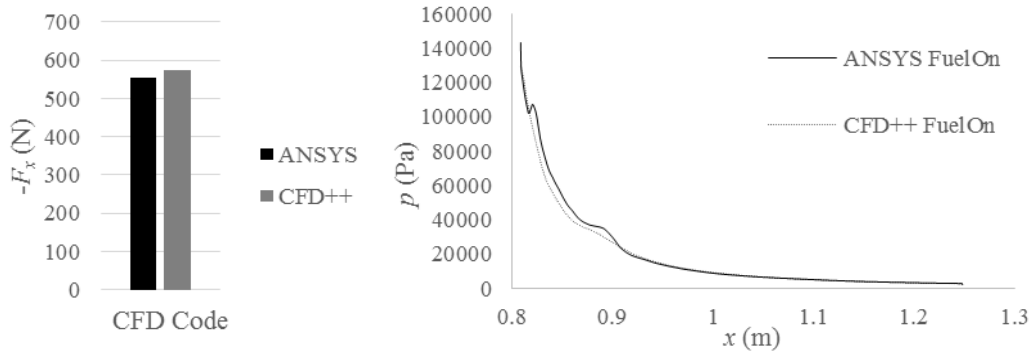

Fig. 6 Comparison of total axial forces between solutions calculated by two different codes (left), comparison of static pressure on the nozzle wall calculated by two different codes (right)

through ANSYS are consistent with those solved in CFD++. Fig. 6 presents the total axial force acting on the nozzle as computed by ANSYS and CFD++; a deviation in total axial force of 3.4% is obtained validating that the scramjet nozzle is accurately modeled by ANSYS. The small discrepancy between the two codes can be attributed to inconsistencies in the meshing and differences in the methods by which each code solves the flowfields. Fig. 6 demonstrates that the static pressure acting upon the nozzle wall is in reasonable agreement for both codes further validating that the scramjet nozzle is accurately modeled by ANSYS. ANSYS appears to have captured a more detailed representation of the flowfield characteristics than CFD++, such as the pressure rise due to the shock impingement just upstream of the nozzle throat and at x=0.9 m.

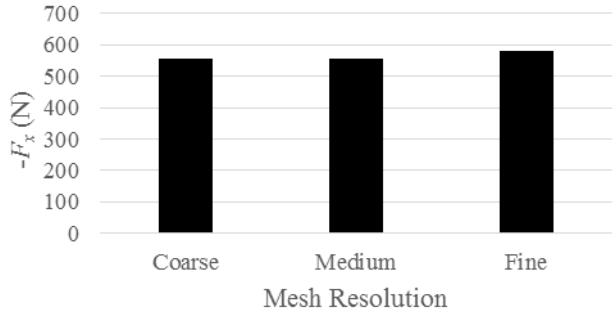

Fig. 7 Comparison of total axial forces for various mesh resolutions

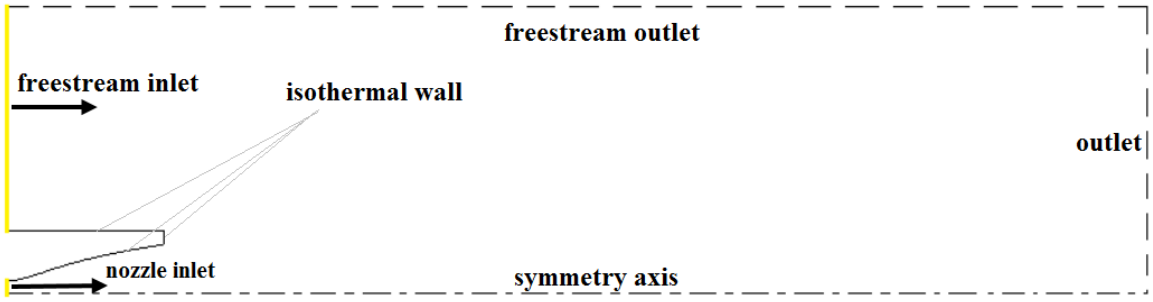

Fig. 8 Boundary conditions

The total axial force on the scramjet nozzle is compared for three levels of mesh resolution. This comparison is made prior to the introduction of the injector. The following resolutions are considered; coarse (32,350 cells), medium (133,911 cells) and fine (533,821 cells). For the fine resolution the mesh density in both axial and radial directions is increased by a factor of 2, for the superfine resolution the mesh density in both radial and axial directions is increased by a factor of 4. Fig. 7 demonstrates that there is not a significant difference between the three resolutions, with a maximum deviation of 4%. For the present parametric study the coarse resolution is implemented.

2.2.4 Flow and boundary conditions

The fixed flow conditions of the injector consider sonic fuel injection (M_j=1) and a static temperature of T_j=250K. The body of the scramjet is considered to comprise of isothermal cold walls at 300K, which is valid for impulse facility or short duration flight testing. The nozzle inflow profiles are obtained from CFD simulations for the nominal SCRAMSPACE specification (Boyce *et al.* 2011) and are presented in Fig. 9. Pressure far-fields are imposed on the freestream, nozzle and injector inlets while the upper and downstream boundaries are set as pressure outlets as presented in Fig. 8. The downstream boundary is set to more than 10 times the nozzle length in order to allow the flow to recover to freestream conditions.

2.3 Parameters

For the present parametric study, the injection pressure p_j, injection angle θ_j and streamwise injection position x_j as a fraction of the nozzle length l_n are modified according to Table 3. The injector height h_j is fixed at 2 mm. A parametric representation of the injection is presented in Fig. 10.

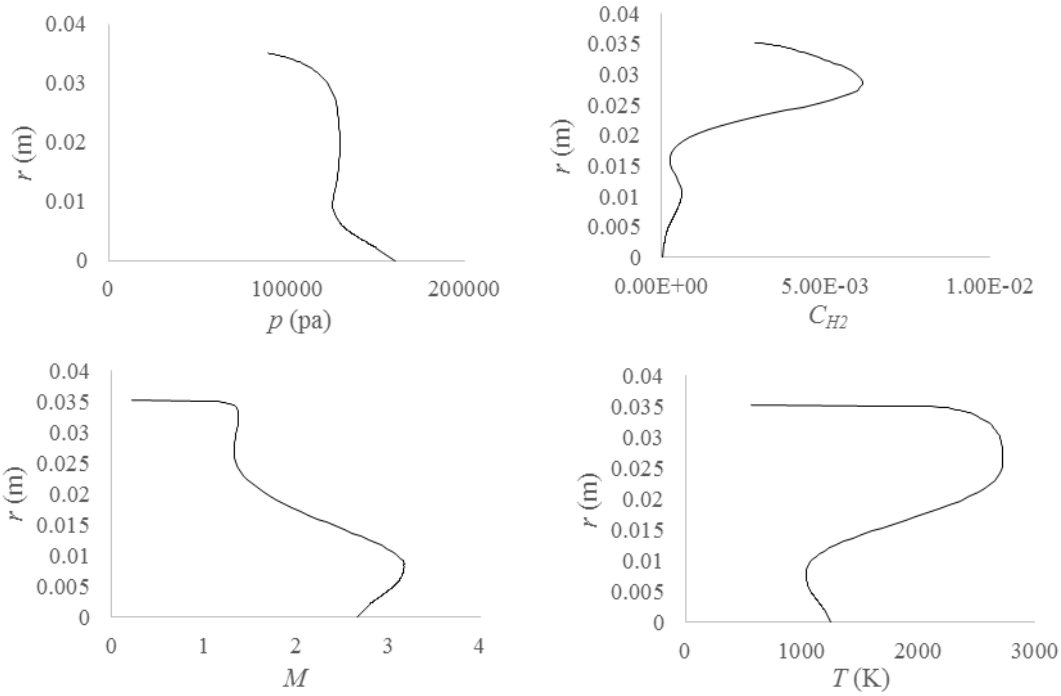

Fig. 9 Inflow profiles of static pressure (top left), hydrogen mass fraction (top right), Mach number (bottom left) and static temperature (bottom right)

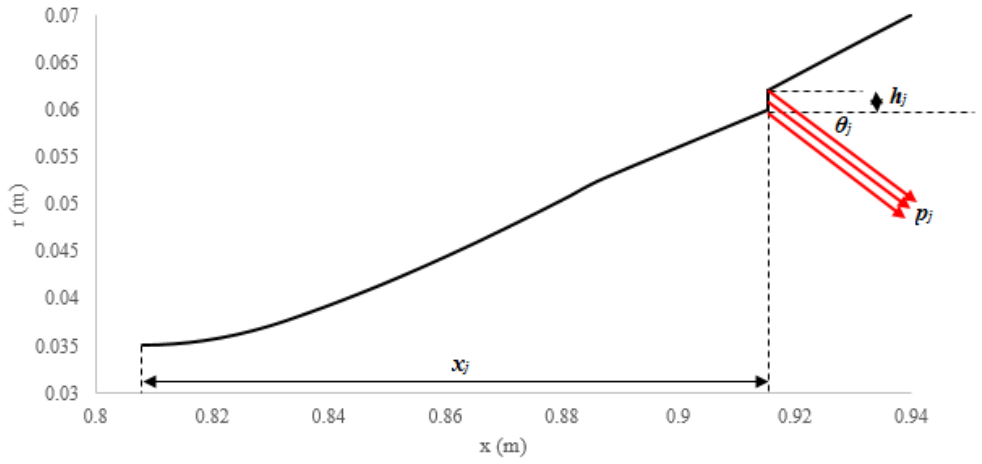

Fig. 10 Parametric representation of the injector

The injection position x_j influences the hydrogen-oxygen mixing and combustion time significantly. As the injector moves downstream of the nozzle entrance, less time will be available for mixing and combustion. With the injector positioned near the nozzle entrance, high static temperatures and pressures will be expected, promoting combustion. The level of penetration that the fuel jet is able to attain is influenced by the injector position due to the high local static

Table 3 Parameters to be used in the parametric study

Distance from Nozzle Throat x_j ($\times l_n$)	Injection Angle θ_j (◦)	Injection Total Pressure p_{0j} (bar)
0.125	0	5
0.25	15	10
0.375	30	15
0.5	45	20
-	60	25

Table 4 Parameters and total thrust for the optimum configuration

Parameter	Optimum Configuration	Baseline Configuration
x_j [m]	0.375	-
θ_j [◦]	30	-
p_{0j} [bar]	25	-
F_x [N]	**2233**	**554**

pressures of the crossflow, it is expected that as the injector moves downstream of the nozzle entrance, sufficient penetration will occur at lower injection pressures however the local static temperatures and pressures will be lower and less time will be available for mixing. As the injector height h_j is fixed the mass flow rate of fuel $\dot{m}_j$ will increase as the injector moves downstream (due to the increased area of the injection annulus), this phenomenon will further augment thrust.

Injection pressure p_j and injection angle θ_j influence the penetration levels of the fuel jet such that at higher pressures and angles higher levels of penetration occur and allow for enhanced hydrogen-oxygen mixing. The momentum produced by the fuel jet also directly influences the augmentation of thrust such that higher injection pressures yield a greater momentum increase. There is expected to be a prominent interaction between the fuel jet and the cross-flow causing a bow shock which is intensified with higher pressures and angles, this causes upstream and downstream wall flow separation and increased static wall temperatures (Drummond *et al.* 2006).

3. Results

3.1 Total axial force

The total axial force F_x acting on the nozzle is calculated including the contribution of viscous and inviscid forces acting on the nozzle and exterior walls. It is found that the total injection pressure is the dominating factor when considering the level of thrust augmentation that can be attained, such that higher injection pressures lead to higher levels of thrust augmentation. Table 4 presents the combination of parameters which are found to be optimum, inducing the highest total axial force in comparison to the baseline geometry.

It is found that at θ_j=30° the greatest level of thrust augmentation is obtained. For injection angles less than this sufficient penetration does not occur and for steeper injection angles the losses incurred due to intensified levels of interaction between the fuel jet and the cross-flow causing upstream and downstream flow separation become too significant and surpass the enhanced levels of penetration.

At x_j=0.375l_n maximum levels of thrust augmentation are observed. With the injector closer to the nozzle throat sufficient penetration is more difficult to attain due to the high pressure of the crossflow. As the injector moves further downstream of the nozzle throat lower static temperatures and pressures of the crossflow are observed which leads to insufficient combustion. Contour plots displaying the variance in total axial force with injection pressure, injection angle and streamwise injection position are presented in Figs. 11-13.

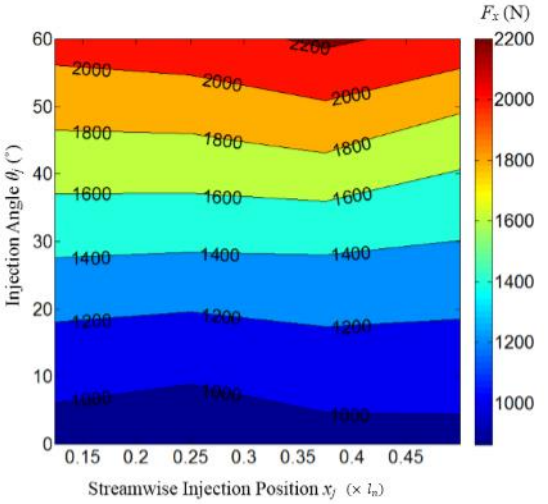

Fig. 11 Total axial force contour plot for injection total pressure of 25 bar with respect to injection angle and streamwise injection position

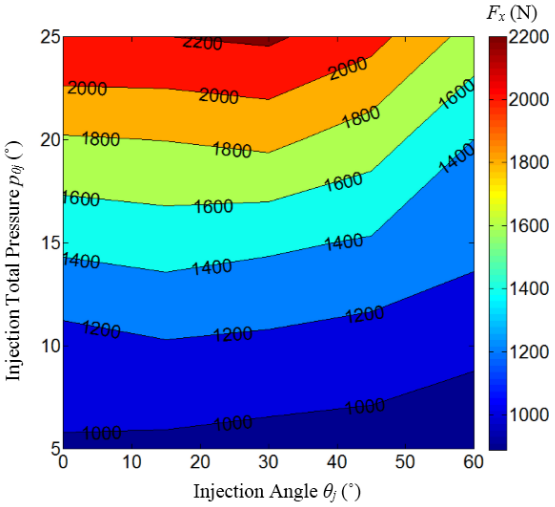

Fig. 12 Total axial force for a streamwise injector position of 0.375 with respect to injection total pressure and injection angle

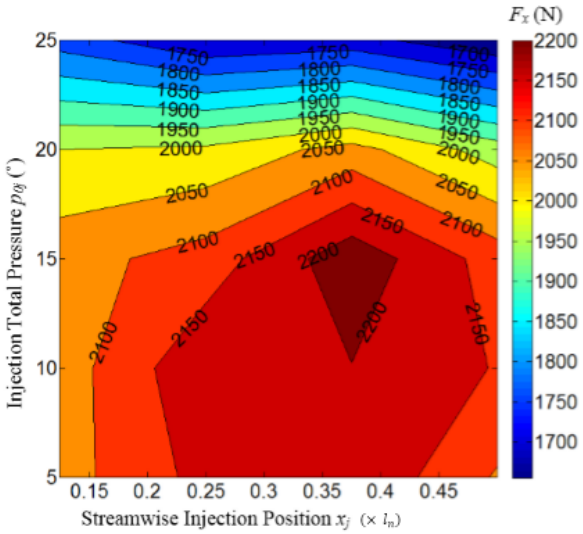

Fig. 13 Total axial force contour plot for an injection angle of 30° with respect to injection total pressure and streamwise injector position

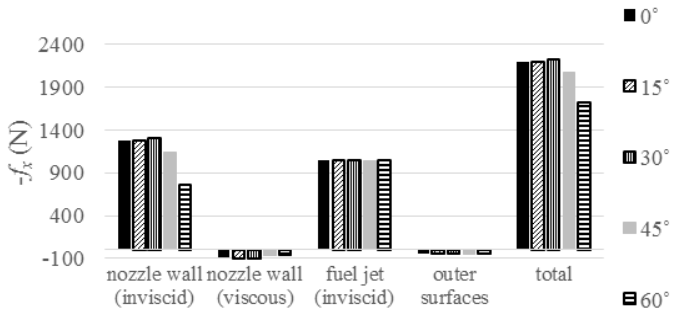

Fig. 14 Force breakdown of axial force components (x_j=0.375, p_{0j}=25 bar) with injection angle variation

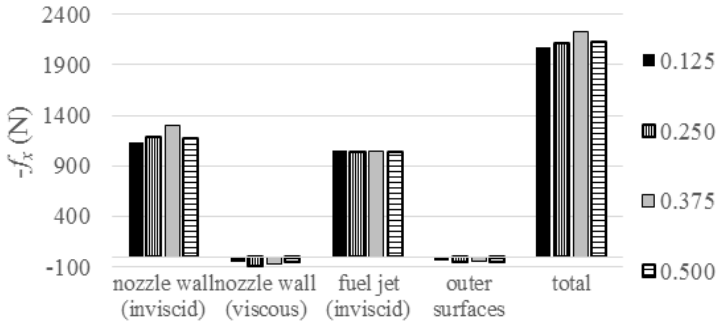

Fig. 15 Force breakdown of axial force components (θ_j=30˚, p_{0j}=25 bar) with injection position variation

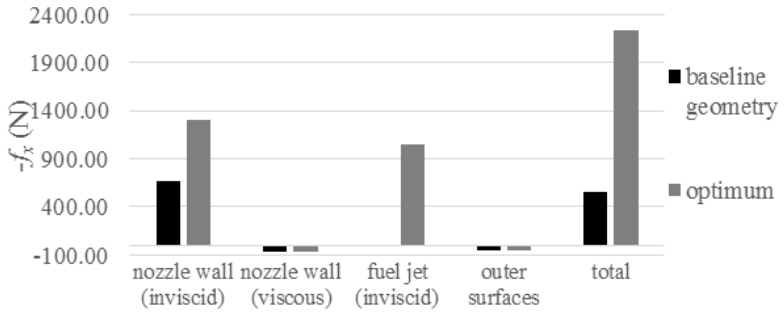

Fig. 16 Force breakdown of axial force components for baseline and optimum cases

3.2 Force breakdown

In order to determine the source of axial forces, Figs. 14-16 and Tables 5-7 present a breakdown of the inviscid, viscous and jet force contributions. The total axial force is significantly dominated by the inviscid force acting on the nozzle wall (thrust). There is also a significant contribution to inviscid force that can be attributed to the momentum increase caused by the fuel jet and a small contribution attributed to the inviscid force on the nozzle base. Whilst viscous (drag) forces on the nozzle and freestream wall are present, they are significantly overpowered by the inviscid forces.

Table 5 Force breakdown of axial force components (x_j=0.375, p_{0j}=25 bar) with injection angle variation

Injection Angle (˚)	Nozzle Wall (Inviscid) (N)	Nozzle Wall (Viscous) (N)	Fuel Jet (N)	Outter Surface (N)	Total (N)
0	1282.01	-85.92	1045.58	-46.04	2195.63
15	1275.56	-76.76	1045.58	-46.04	2198.33
30	1302.50	-68.80	1045.58	-46.04	2233.23
45	1135.31	-65.46	1045.58	-46.04	2069.39
60	771.17	-51.79	1045.58	-46.04	1718.92

Table 6 Force breakdown of axial force components (θ_j=30˚, p_{0j}=25 bar) with injection position variation

Streamwise Injection Position (×l_n)	Nozzle Wall (Inviscid) (N)	Nozzle Wall (Viscous) (N)	Fuel Jet (N)	Outter Surface (N)	Total (N)
0.125	1135.71	-55.23	1045.58	-46.04	2080.01
0.250	1192.29	-70.26	1045.58	-46.04	2121.
0.375	1302.50	-68.80	1045.58	-46.04	2233.23
0.500	1179.50	-51.81	1045.58	-46.04	2127.23

Table 7 Force breakdown of axial force components for baseline and optimum cases

	Nozzle Wall (Inviscid) (N)	Nozzle Wall (Viscous) (N)	Fuel Jet (N)	Outter Surface (N)	Total (N)
Baseline	665.32	-59.57	0.00	-51.51	554.24
Optimum	1302.50	-68.80	1045.58	-46.04	2233.23

Fig. 16 demonstrates the level of thrust augmentation that is produced when comparing the optimum injection configuration with the baseline geometry. It is apparent that a significant portion of the thrust augmentation is attributed to the momentum increase by the fuel jet, the energy required to achieve this momentum is likely to significantly counteract the net gain in thrust and thus it is likely that the net thrust is not as pronounced as indicated, quantifying and addressing this matter is a prospect for future work.

3.3 Nozzle flow fields

Flowfields for Mach number and hydrogen mass fraction are produced comparing the cases of baseline geometry and optimum injection configuration which are presented in Figs. 17-18. Observation of Fig. 17 indicates that the oxygen jet is achieving substantial penetration into the crossflow leading to combustion of the remaining hydrogen and with enhanced mixing the level of combustion is expected to amplify. Fig. 18 indicates the considerable effects of oxygen injection on the crossflow, where a prominent bow shock is formed due to interactions between the fuel jet and crossflow followed by expansion in the separated region downstream. Reflection of the shock can be observed at approximately x_j=1 m followed by an impingement on the nozzle wall between x_j=1.1 and 1.2 m causing further expansion.

Whilst combustion is observed, the phenomenon is not as significant as expected. This is assumed to be attributed to inadequate mixing as well as little occurrence of ignition due to insufficient temperatures and pressures as the injection position moves downstream of the nozzle

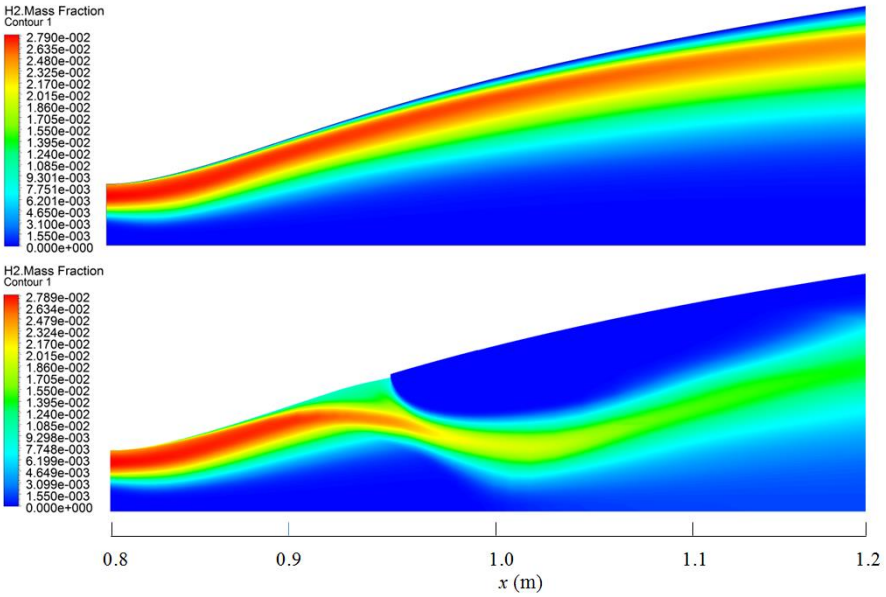

Fig. 17 Hydrogen mass fraction distributions for baseline geometry (top) and optimum injection case (bottom)

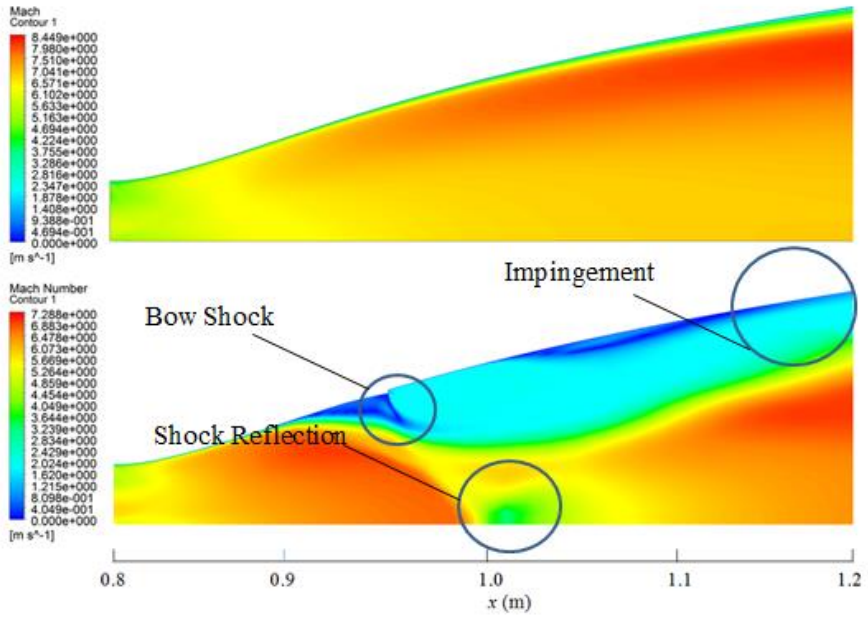

Fig. 18 Mach number distributions for baseline geometry (top) and optimum injection case (bottom)

throat. The axisymmetric nature of the problem makes a significant contribution to the current inadequate mixing. In order to enhance the mixing and combustion, the turbulence, reaction and diffusivity models shall be examined and revised in a future study.

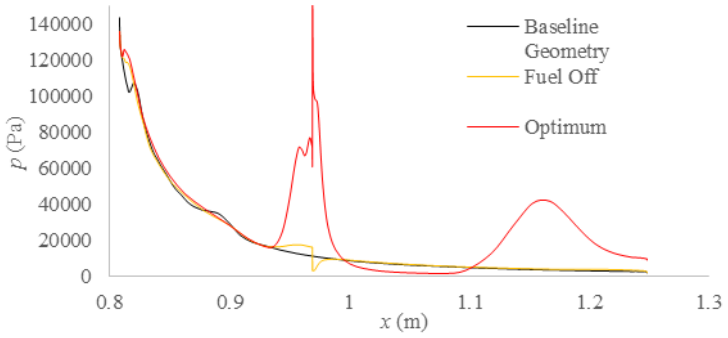

Fig. 19 Surface pressure distributions

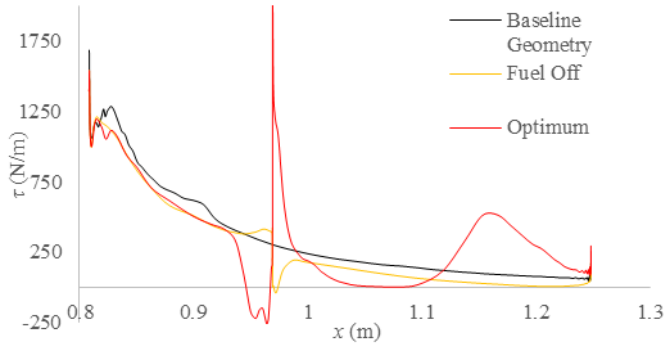

Fig. 20 Shear stress distributions

3.4 Surface forces

The axial forces acting on the nozzle surface were attained by integrating the pressure, p, and shear stresses, τ_x, as presented in Eq. (1)

$$\begin{aligned} F_x &= F_{x\,inviscid} + F_{x\,viscous} \\ &= \int_{r_i}^{r_0} 2\pi r p dr \int_0^{l_n} 2\pi r \tau_x dx \\ &= 2\pi r \left(\int_{r_i}^{r_0} p dr \int_0^{l_n} \tau_x dx \right) \end{aligned} \tag{1}$$

where, r_i, r_o and l_n represent the nozzle inlet radius, nozzle outlet radius and nozzle length respectively.

The surface pressure and shear stress distributions, presented in Figs. 19-20, indicate that the introduction of the injector geometry, without fuel injection, leads to a shock occurring in the region of the injection wedge. Inspection of the case of the optimum injection configuration indicates a significant increase in surface pressure in the region of the injection point. This is followed by a small drop in surface pressure downstream due to expansion then a significant increase just upstream of the nozzle exit which can be attributed to the reflection of the shock in

the axisymmetric configuration; a total presure increase of 2857 Pa is achieved. The shear stress distributions demonstrate similar behaviour and an increase of 70 N/m is observed. The main source of thrust augmentation appears to be occurring due to the extreme surface pressure increases that are observed in the injection region and at the nozzle exit. The increase in shear stress on the nozzle wall is not found to be significant as the increase in surface pressure is by far dominant.

4. Conclusions

A parametric study has been conducted using numerical methods to investigate thrust augmentation through supersonic afterburning in scramjet engine nozzles. 100 numerical simulations were conducted investigating the effect of different configurations of three parameters on thrust augmentation. These parameters included the streamwise injection position, injection pressure and injection angle.

As might be expected, a high correlation was found between thrust augmentation and injection pressure such that at higher injection pressures higher levels of thrust augmentation were attained. For the optimum injection configuration the total thrust acting upon the nozzle was found to increase considerably in comparison to the baseline geometry. Observation of the force breakdown demonstrates that the thrust augmentation is due to the contribution of both inviscid forces acting upon the nozzle wall and increased momentum due to the fuel jet.

Comparison of the hydrogen mass fraction flowfields for the optimum injection configuration and baseline geometry indicate that less hydrogen remains at the nozzle outlet with the occurrence of injection, indicative of hydrogen combustion. The surface pressure acting on the nozzle wall was found to significantly increase in the region of the injection point and at the nozzle exit leading to a surface pressure increase of 125% when comparing the optimum injection configuration to the baseline geometry. This pressure increase is one of the main sources of thrust augmentation. A similar occurrence was observed for the shear stress acting upon the nozzle wall. However, the increase in shear stress was found to be less than 1% of the surface pressure increase and therefore was considered negligible. The complex phenomenon associated with the aerodynamics and chemical reactions in the scramjet nozzle introduced a scenario where an optimum configuration requires a fine balance between the parameters that are investigated in this paper.

Future work will include an investigation into the enhancement of mixing and combustion through improved turbulence, reaction and diffusivity modeling. This will be followed by a design optimization through surrogate-assisted evolutionary algorithms focusing on minimising the energy associated with fuel injection whilst quantifying and maximizing the thrust increase due to combustion. Finally an alternate injection configuration *i.e.,* strut injector, is also currently being investigated.

References

Boyce, R.R., Tirtey, S.C., Brown, L., Creagh, M. and Ogawa, H. (2011), "SCRAMSPACE: scramjet-based access-to space systems", AIAA Paper 2011-2297, *17th AIAA International Space Planes and Hypersonic Systems and Technologies Conference*, California, USA, April.

Bulman, M. (2006), "Thrust Augmented Nozzle (TAN): the new paradigm for booster rockets", AIAA Paper 2006-4371, *42nd AIAA/ASME/SAE/ASEE Joint Propulsion Conference and Exhibit*, Sacramento, USA, July.

Chan, W.Y.K., Jacobs, P.A. and Mee, D.J. (2012), "Suitability of the k-ω turbulence model for scramjet flowfield simulations", *Int. J. Numer. Meth. Fluid.*, **70**(4), 493-514.

Cutler, A.D., Harding, G.C. and Diskin, G.S. (2001), "High frequency supersonic pulsed injection", AIAA Paper 2001-0517, *39th AIAA Aerospace Sciences Meeting and Exhibit*, Nevada, USA, January.

Davies, M. (2003), *The Standard Handbook for Aeronautical and Astronautical Engineers*, McGraw-Hill, New York, NY, USA.

Davis, R.L., Bulman, M.J. and Yam, C. (2006), "Numerical simulation of a thrust augmented rocket nozzle", AIAA Paper 2006-5205, *42nd AIAA/ASME/SAE/ASEE Joint Propulsion Conference*, Sacramento, USA, July.

Dorrington, G.E. (2002), "Rationale for supersonic afterburning rocket engines", *J. Spacecraft*. **40**(2), 301-303.

Drummond, J.P., Carpenter, M.H. and Riggins, D.W. (1991), *Progress in Astronautics and Aeronautics*, Sunset Books, Newark, OH, USA.

Drummond, J.P., Diskin, G.S. and Cutler, A.D. (2006), *Technologies for Propelled Hypersonic Flight*, Scientific and Technical Aerospace Reports, Hampton, VA, USA.

Evans, J.S. and Schexnayder, Jr., C.J. (1980), "Influence of chemical kinetics and unmixedness on burning in supersonic hydrogen flames", *AIAA J.*, **18**(2), 188-193.

Ferrante, F.A. and Chen F.F. (2006), "Thermal design and analysis of the Thrust Augmented Nozzle (TAN) injector", AIAA Paper 2006-4541, *42nd AIAA/ASME/SAE/ASEE Joint Propulsion Conference and Exhibit*, Sacramento, USA, July.

Ferri, A., Moretti, G. and Slutsky, S. (1965), "Mixing processes in supersonic combustion", *J. Soc. Indus. Appl. Math.*, **13**(1), 229-258.

Forde, S., Bulman, M. and Neill, T. (2006), "Thrust augmentation nozzle (TAN) concept for rocket engine booster applications", *Acta Astronautica*, **59**(1-5), 271-277.

Froning, H.D. (1989), "Investigation of very high energy rockets for future SSTO vehicles", *Acta Astronautica*, **14**(4), 321-320.

Maicke, B.A. and Majdalani, J. (2010), "Evaluation of CFD codes for hypersonic flow modeling", AIAA Paper 2010-7184, *46th AIAA/ASME/SAE/ASEE Joint Propulsion Conference*, Tennessee, USA, July.

Manoha, E., Redonnet, S., Terracol, M. and Guenanff, G. (2004), "Numerical simulation of aerodynamic noise", *4th European Congress on Computational Methods in Applied Sciences and Engineering*, Jyväskylä, Finland, January.

Mary, I. and Sagaut, P. (2002), "Large eddy simulation of flow around an airfoil near stall", *AIAA J.*, **40**(6), 1139-1145.

McClinton, C.R. (2006), "X-43-Scramjet power breaks the hypersonic barrier dryden lectureship in research for 2006", AIAA Paper 2006-1, *44th AIAA Aerospace Sciences Meeting and Exhibit*, Nevada, USA, January.

Mutzman, R. and Murphy, S. (2011), "X-51 development: a chief engineer's perspective", *17th AIAA International Space Planes and Hypersonic Systems and Technologies Conference*, San Francisco, USA, April.

Ogawa, H. and Boyce, R.R. (2012), "Nozzle design optimisation for axisymmetric scramjets by using surrogate-assisted evolutionary algorithms", *J. Propul. Pow.*, **28**(6), 1324-1338.

Pandey, K.M. and Sivasakthivel, T. (2011), "CFD analysis of mixing and combustion of a scramjet combustor with a planer strut injector", *Int. J. Environ. Sci. Develop.*, **2**(2), 102-108.

Papamoschou, D. and Roshko, A. (1986), "Observation of supersonic free shear layers", AIAA Paper 1986-0162, *AIAA 24th Aerospace Sciences Meeting*, Nevada, USA, January.